Effect of Tungsten on Long-Term Microstructural Evolution and Impression Creep Behavior of 9Cr Reduced Activation Ferritic/Martensitic Steel

V. THOMAS PAUL, V.D. VIJAYANAND, C. SUDHA, and S. SAROJA

The present study describes the changes in the creep properties associated with microstructural evolution during thermal exposures to near service temperatures in indigenously developed reduced activation ferritic-martensitic steels with varying tungsten (1 and 1.4 wt pct W) contents. The creep behavior has been studied employing impression creep (IC) test, and the changes in impression creep behavior with tungsten content have been correlated with the observed microstructures. The results of IC test showed that an increase in 0.4 pct W decreases the creep rate to nearly half the value. Creep strength of 1.4 pct W steel showed an increase in steels aged for short durations which decreased as aging time increased. The microstructural changes include coarsening of precipitates, reduction in dislocation density, changes in microchemistry, and formation of new phases. The formation of various phases and their volume fractions have been predicted using the JMatPro software for the two steels and validated by experimental methods. Detailed transmission electron microscopy analysis shows coarsening of precipitates and formation of a discontinuous network of Laves phase in 1.4 W steel aged for 10,000 hours at 823 K (550 °C) which is in agreement with the JMatPro simulation results.

I. INTRODUCTION

MICROSTRUCTURAL stability on prolonged thermal exposure is an essential criterion for the 9Cr reduced activation ferritic-martensitic (RAFM) steels, the structural material selected for the test blanket module in the International Thermonuclear Experimental Reactor (ITER). The severe operating conditions impose stringent requirements on properties, especially with respect to embrittlement and degradation of high-temperature strength due to microstructural evolution.[1] Prolonged thermal exposure of the tempered martensite structure leads to continuous evolution of secondary phases and substructure changes in the RAFM steels. Although the principal carbide in this steel is $M_{23}C_6$, small amounts of carbonitrides of V and Ta also form during tempering. Further precipitation, coarsening, and spheroidization of carbides occur during aging or under creep conditions. The changes include coarsening of precipitates, reduction in dislocation density, changes in microchemistry, and formation of new phases. 9Cr-1Mo steels and its variants being a workhorse of petrochemical and energy industries, the above aspects have been studied by several research groups all over the world.[2–4]

Addition of tungsten to the steel is beneficial as it produces a more stable microstructure that resists recovery of martensite by stabilizing the initial dislocation substructure. It also enhances the high-temperature strength by increasing the binding force among the atoms in solid solution. Alloying elements such as W and Ta exert a profound influence on the kinetics of different processes like formation, dissolution, and coarsening of precipitates. It is reported that in 9Cr steels, tungsten refines the martensitic lath size and resists its coarsening during creep exposure.[5,6] Additionally, the presence of tungsten in carbides reduces its coarsening kinetics by retarding self-diffusion of iron.[7] The role of W and Ta in refining the prior austenite grain size in 9Cr RAFM has also been reported.[8] Furthermore, W is found to be more effective in resisting the recovery of martensite than Ta. Prolonged exposure to high temperatures produces Laves phase (Fe_2W) and its volume fraction depends on W content in the steel. But formation of Laves on long-time service temperatures is known to deteriorate the creep properties.[9,10]

In the present study, impression creep (IC) is used to compare the creep properties of RAFM steels with two different tungsten contents of 1 wt pct W and 1.4 wt pct W (termed as INRAFM).[11] Further, the change in property is also corroborated with the microstructural evolution in these steels during prolonged thermal exposure at near service temperatures. Although the

V. THOMAS PAUL, Scientific Officer 'F', V.D. VIJAYANAND, Scientific Officer 'D', C. SUDHA, Scientific Officer 'F', and S. SAROJA, Head, MTPD, Professor, are with the Metallurgy and Materials Group, Homi Bhabha National Institute, Indira Gandhi Centre for Atomic Research, Kalpakkam, Tamil Nadu, 603 102, India. Contact e-mail: saroja@igcar.gov.in
Manuscript submitted April 8, 2016.
Article published online October 26, 2016.

creep behavior of RAFM steels is dealt with in several publications,[6,12–14] there is limited information on the combined influence of high-energy neutron flux, temperature, and stress. Under this backdrop, the present study aimed at generating the out of pile data under similar thermal exposure and testing conditions. Hence, it was necessary to employ small specimen test methods for a comparative study with the irradiated steel. Evaluation of creep properties of the aged steel employing a high load for short-time duration prevents microstructural changes in the steel during testing. Hence, the use of impression creep testing technique was most appropriate as the steady-state creep rate could be obtained within a short span of time.

II. EXPERIMENTAL

9Cr RAFM steels with 1 and 1.4 wt pct of tungsten supplied by M/s MIDHANI, Hyderabad in the form of 12-mm thick plates (normalized at 1253 K (980 °C)/1 hour and tempered at 1033 K (760 °C)/1 hour) have been used in the present study. Chemical composition of the two steels is given in Table I. Specimen cut from the plates were encapsulated in vacuum-sealed quartz tubes and aged at 773 K (500 °C) and 823 K (550 °C) for durations of 5000 and 10,000 hours, to study the long-term microstructural behavior.

Standard polishing and etching techniques were used for metallographic preparation of specimens. Vickers microhardness measurements at a load of 100 g were carried out using a Leitz Miniload-2 microhardness tester. Scanning electron microscopy (SEM) was carried out using Philips XL-30 and Analytical transmission electron microscopy (ATEM) was carried out using a Philips CM 200 microscope at an operating voltage of 120 to 200 kV equipped with Oxford X-max SDD detector for microstructural and microchemical analysis. Low-magnification micrographs from extraction replica were used to determine the volume fraction and size distribution of secondary phases by employing image analysis software 'ImageJ.' The size of the precipitate is quoted in terms of normalized diameter, which was calculated from the projected area of the particle assuming it as globular in shape. In general, $M_{23}C_6$ carbides showed a wide range of size, but MX was found to be fine in nature. Due to this wide variation, size of the precipitate is presented as a frequency distribution plot. However, for volume fraction analysis, no distinction could be made between the two types of carbides, due to very low fraction and size of MX. The volume fraction of the precipitates has been calculated based on area fraction analysis of several regions from a large number of images from the extraction replica. However,

it is necessary to mention that the microscopic undulations in the etched surface cause errors in the analysis, which is due to extraction of stray precipitates from planes below the surface of the specimen.[15]

JMatPro® simulation software was used extensively to determine the change in phase constitution as a function of composition and temperature. JMatPro® employs a CALPHAD-based database for the computation of thermodynamic properties. Equilibrium phases were identified by thermodynamic calculations using Gibb's energy minimization routines proposed by Kattner et al. and Lukas et al.[16,17] Based on the equilibrium calculations, phase stability, phase fraction, and composition of each phase were determined for different temperature domains.

A. Impression Creep Test

In impression creep (IC) test, a constant load is applied to the test specimen of thickness 10 mm through a flat-bottomed cylindrical indenter of 1 mm diameter, made of tungsten carbide. The sample is machined parallel to surface and ground to 1 μm finish. The experiment is carried out at a vacuum level of 10^{-6} mbar in order to avoid oxidation of the indenter and the specimen. The temperature is controlled within ±1 K (1 °C). The punch penetration depth was recorded as function of test time using a LVDT with an accuracy of ±1 μm. A typical test results that show total deformation vs time for different stress levels are provided in Figure 1. The punching stress (σ_{imp}) and impression velocity in impression creep test can be directly correlated to uniaxial stress (σ_{uni}) and uniaxial creep rate ($_{uni}$) by using suitable parameters. The material during impression creep test is reported to exhibit the same stress and temperature dependence as the stress in a conventional tensile creep test.[18] IC tests can therefore be used to produce reliable creep strain rates, equivalent to those obtained from a normal creep test. In this study, impression creep tests were carried out at 823 K (550 °C), which is the highest limit of service temperature for ferritic-martensitic steels.

III. RESULTS

A. Microstructural Characterization of Normalized and Tempered Steels

The 1 and 1.4 W (designated as Indian RAFM or INRAFM) steels exhibited a tempered martensite structure typical of normalized and tempered ferritic-martensitic steels. The average prior austenitic grain size (PAGS) was measured as 14 and 10 μm in the 1 W and INRAFM steels, respectively. Average hardness of

Table I. Chemical Composition (in Weight Percent) of the Two RAFM Steels Used in this Study

Steel	Cr	C	Mn	V	W	Ta	N	O	P	S	Ti	Ni	Mo	Nb
1 W	9.04	0.08	0.55	0.22	1.0	0.06	0.022	0.005	<0.002	<0.002	0.005	0.005	0.001	0.001
INRAFM	9.03	0. 12	0.56	0.24	1.39	0.06	0.029	0.002	<0.002	<0.001	0.005	0.005	0.002	0.001

~230 and ~240 VHN for the 1 W and INRAFM steels is in agreement with the tempered martensite structure with a slightly higher value in INRAFM due to higher W content. Figure 2 shows the TEM thin foil micrographs of normalized and tempered 1W RAFM steel. A large number of dislocations and retention of lath morphology, in the prior austenite grains are clearly shown in Figure 2(a). The laths are decorated with carbides of various sizes, predominantly of lenticular morphology, as shown in Figure 2(b). Figure 3 shows the details of the phases from carbon extraction replica of the 1 W steel. The distribution of precipitates along lath boundaries is shown in Figure 3(a). Diffraction patterns from two typical precipitates are shown in the inset of Figure 3(a) (diffracting planes are marked). Analysis of these patterns and comparison with standard values of d-spacing the phases were identified as $M_{23}C_6$ and MX precipitates (M stands for metal atoms and X stands for C or N). Energy-dispersive spectrum (EDS) from these precipitates showed that the former was 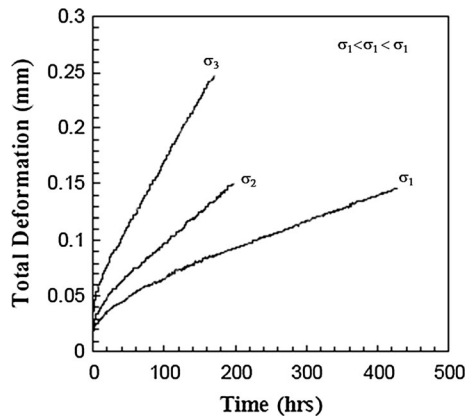rich in Cr, while the latter was V/Ta-rich. Similar results were obtained for the INRAFM steel also. A higher volume fraction of carbides was observed in INRAFM (0.035 V_f) as compared to 1 W steel (0.018 V_f), which is attributed to the higher carbon content in the steel. In general, the presence of $M_{23}C_6$ was more dominant than MX. In contrast, MX carbides were few and of very fine size in the range from 10 to 15 nm. Size distribution of $M_{23}C_6$ carbides (Figure 3(c)) showed a Gaussian distribution of 50 to 130 nm in both the steels.

B. *Microstructure of Normalized and Tempered Steel: Computation*

The volume fraction, size, and microchemistry of secondary phases at different temperatures were simulated using 'JMatPro.' The change in phase fraction as a function of temperature until melting point was computed for the two steels and the results of 1 W RAFM steel are depicted in Figure 4(a). The equilibrium phases predicted in the temperature range of interest [1000 K (727 °C) −1253 K (980 °C)] showed the formation of $M_{23}C_6$, MX, ferrite, and austenite. Dissolution temperature of $M_{23}C_6$ was found to be higher in INRAFM than in 1 W steel.[19] The change in phase fraction with time at a temperature of 1033 K (760 °C) for 1W RAFM steel is given in Figure 4(b). It is seen from the plot that tempering for 1 hour results in the precipitation of predominantly $M_{23}C_6$ with few MX carbides, which is in agreement with the experimental observation (Figure 3(b)). The partitioning of W and Ta among various phases in 1W RAFM steel is shown in Figures 4(c) and (d), respectively. The presence of W in both ferrite and $M_{23}C_6$ phases suggests that W not only acts as ferrite stabilizer but also provides enhanced solid solution strengthening and precipitation hardening. Tungsten also has a tendency to promote Laves phase formation as reported in the literature.[20] But Ta primarily evolves into MX type of precipitates. Laves phase also has some solubility for Ta.
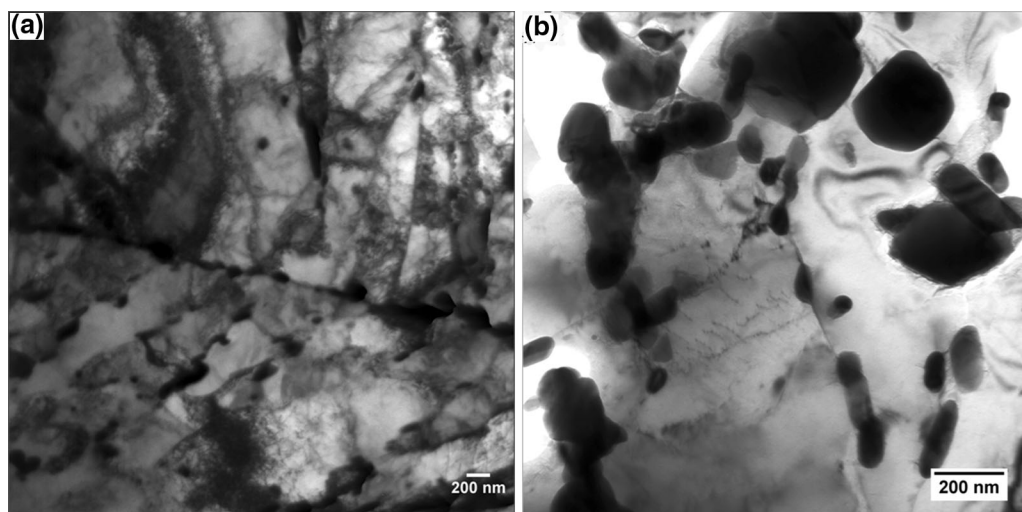

Fig. 1—Typical test results of impression creep—total deformation *vs* time—for different stress levels.

Fig. 2—Bright-field TEM micrograph of normalized and tempered 1W RAFM steel showing (*a*) decoration of precipitates on lath boundaries in two adjacent prior austenite grains and (*b*) variation in size and shape of carbides.
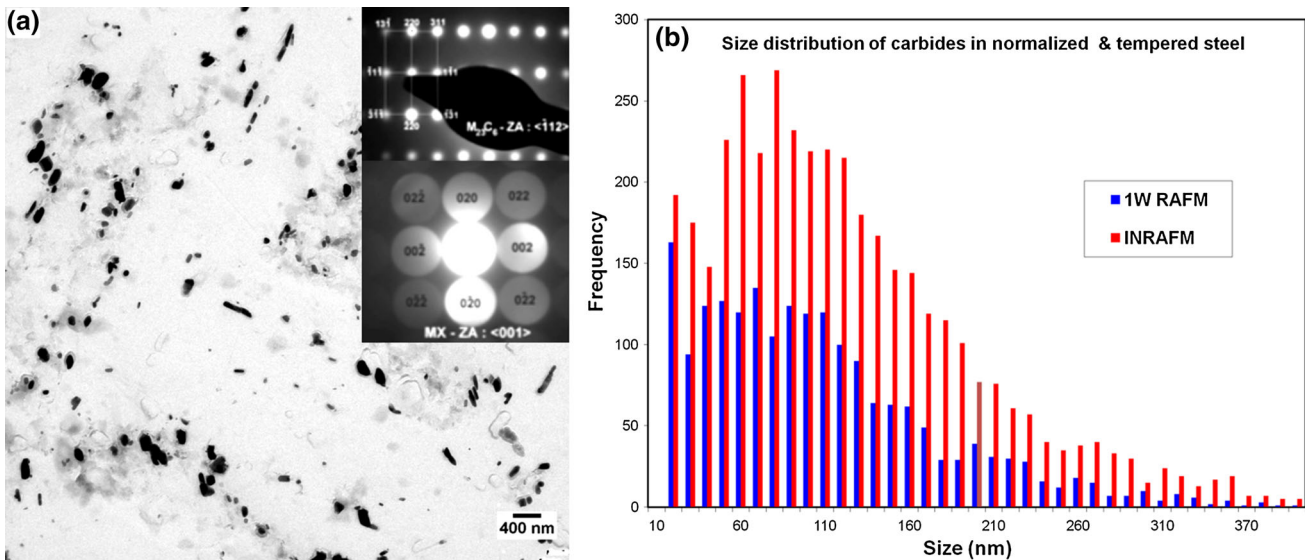
Fig. 3—TEM micrograph of carbon extraction replica of normalized and tempered RAFM steel showing (*a*) inter- and intra-lath boundary carbides in 1 W steel (inset—showing diffraction patterns from $M_{23}C_6$ and MX along $\langle\bar{1}12\rangle$ and $\langle001\rangle$ zone axes, respectively) and (*b*) carbide size distribution in 1 W and INRAFM steels.

C. Studies on Creep Behavior of RAFM Steel by Impression Creep Tests

Impression creep technique is useful for evaluating mechanical properties in a short span of time. Since the steels were aged to considerably longer times, rapid characterization of mechanical properties using impression creep (IC) tests has been carried out. In this section, the results of the IC tests are discussed and correlated with conventional creep data reported in the literature. Creep properties of two steels with different W contents are compared with respect to steady-state creep. Further, effect of microstructural degradation due to thermal aging on creep is also evaluated.

1. Effect of W on creep strength

Impression test was carried out at 823 K (550 °C) on 1 W and INRAFM steels under a punching stress of 787 MPa. Figure 5(a) shows the plot of displacement versus time for both the steels. Testing of the normalized and tempered steels showed a negligible primary creep region. Primary creep also termed as transient creep in which the resistance to deformation of the material increases due to work hardening giving rise to a decreasing creep rate. Table II shows the comparison between the steady-state creep of normalized and tempered 1 W and INRAFM steels. The higher values of secondary creep rates obtained from impression tests than those from conventional tests are understood in terms of the minimum creep rate in the later stages of creep test, just before onset of tertiary creep after which recovery dominates in the conventional case unlike in IC. However, it is evident from the values that the creep rate reduces to nearly half the value with an increase of 0.4 pct W in INRAFM steel.

2. Effect of aging on creep strength

The displacement and creep rate of heat-treated INRAFM steel are shown in Figures 5(a) and (b), respectively. All thermally aged steels showed a distinct primary creep stage unlike normalized and tempered steel. The INRAFM steel which is aged at 773 K (500 °C) for 5000 hours showed the highest depth of penetration as well as highest creep rate. The steady-state impression creep rate remained almost the same for the steel aged for 10,000 hours. On the contrary, the INRAFM steel aged at 823 K (550 °C) for 5000 hours showed the lowest creep rate (corresponds to highest creep strength) among all the aged steel, despite the higher substructure changes expected on exposure to higher temperature. However, an increase in aging time (10,000 hours) at 823 K (550 °C) increased the creep rate to nearly that at 773 K (500 °C)/5000 hours.

3. Change in substructure of region under indentation

The evolution of substructure during indentation was studied using optical, SEM, and Orientation Imaging Microscopy (OIM). The samples which showed the highest (aged at 773 K (500 °C) for 10,000 hours) and lowest (normalized and tempered) creep rate were chosen for this study. The impression creep tested specimen was sectioned along the diameter of the indentation and electropolished for OIM studies. Microhardness measurements were made on the sectioned surface beneath the impression creep indentation. Electron backscattered diffraction (EBSD) analysis was carried out in the region just beneath the indentation mark in order to study the change in morphology and orientation of the ferrite grains due to the deformation process. For a better resolution, EBSD scan was carried out in an area of 800 μm × 400 μm with a step size of 0.6 μm. Figures 6(a) and (b) show the inverse pole
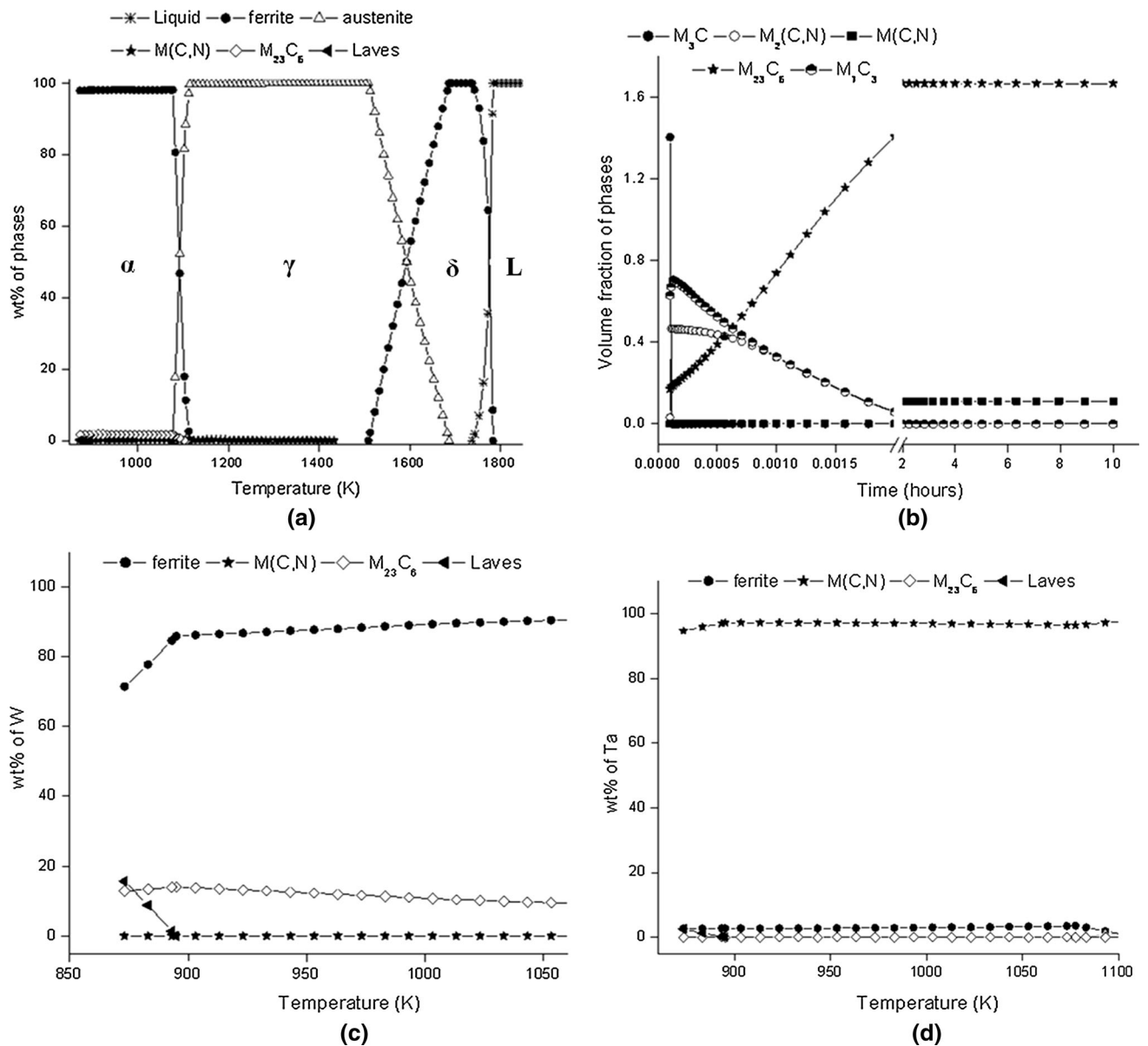
Fig. 4—Computation of equilibrium phases and composition in 1 W steel using 'JMatPro' (*a*) distribution of various phases as a function of temperature (*b*) change in phase (weight) percentage as a function of tempering time at 1033 K (760 °C) (*c*) relative distribution of W and (*d*) Ta in different phases as a function of temperature.

figure map (along horizontal-Y) of the region below the indentor in *n & t* and 823 K (550 °C)/10,000 hours aged INRAFM steel. Three distinct regions (marked I, II, and III in Figure 6(a)) with distinct microscopic features could be observed in the impression-tested samples. Region I which is immediately below the punch did not show any significant change in the morphology of the grains. This shows that the impression creep deformation is localized in nature. Region II exhibited a near hemispherical shape and showed signatures of extensive shear deformation. Region III far away from the indentation showed little change in the shape of the grains.

The orientation of grains along different crystallographic directions as per the legend indicates that there is no preferred orientation. As observed in the optical

micrograph, EBSD also showed three distinct regions. Region II which had undergone extensive deformation also showed two discrete features: (i) elongated grains and (ii) fine grains. It is seen that the elongated (deformed) grains are predominantly oriented along the close-packed ⟨111⟩ and ⟨100⟩ direction. The presence of fine grains can be attributed to the dynamic recovery and recrystallization to some extent. The microhardness measurements across the cross section showed a small increase of 20 VHN in Region II, due to dynamic recovery. Region II was found to be at a depth of ~200 μm for normalized and tempered steel, while for aged steel, elongated regions appeared at a depth of ~400 μm. Also the spread of Region II was found to be more in the case of aged steel. The above observations are due to the relatively soft structure of aged steel as
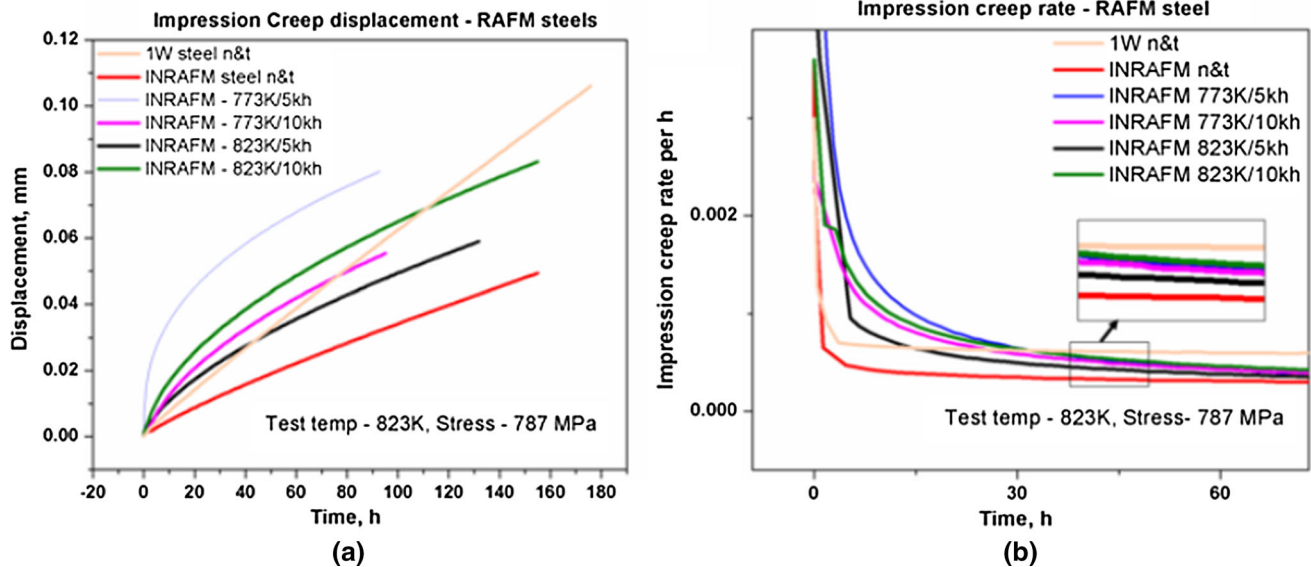
Fig. 5—(*a*) Impression displacement versus time curves and (*b*) impression creep rate for 1 W and INRAFM steels.

Table II. Comparison of Creep Rate Evaluated by Uniaxial Creep Test and Impression Test

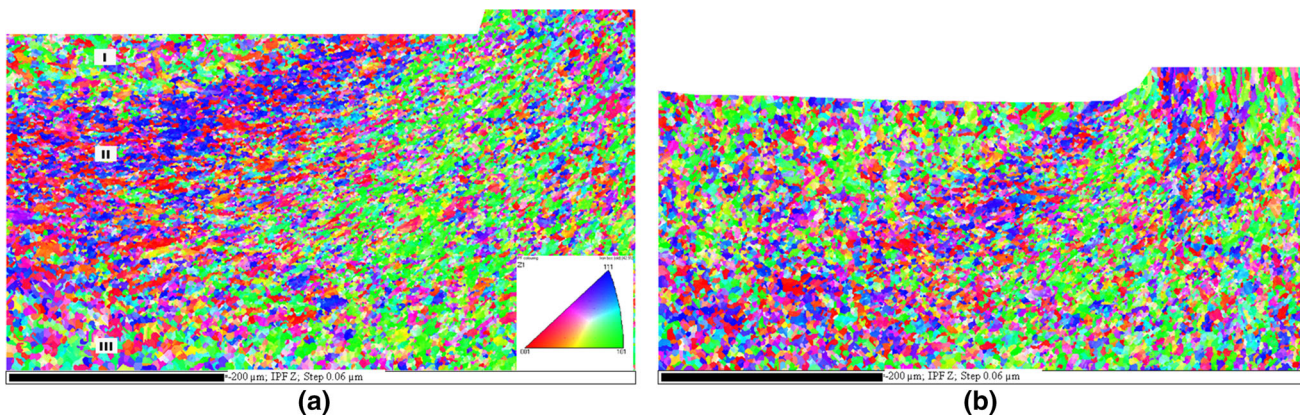| Steel (*n* & *t*)	Uniaxial Creep Test $T = 823$ K (550 °C) and Stress = 220 MPa	Impression Creep Test $T = 823$ K (550 °C) and Stress = 787 MPa
1 W	6.018×10^{-5} h^{-1}	5.86×10^{-4} h^{-1}
INRAFM	1.8×10^{-5} h^{-1}	2.97×10^{-4} h^{-1}

Fig. 6—EBSD crystal orientation maps (standard IPF) from region below indention in (*a*) normalized and tempered and (*b*) aged for 10,000 h at 773 K (500 °C). Three distinct regions are marked where I and III show no significant change, while Region II shows signatures of extensive deformation.

also supported by hardness measurements discussed later. Since the observed creep properties are manifestations of microstructural modifications, the changes in the microstructure during aging were studied in detail by electron microscopy supported by computations.

D. Thermal Exposure Induced Microstructural Evolution in RAFM Steel

A detailed microstructural and microchemical characterization of the phases that form on long-term exposure of RAFM steels (5000 and 10,000 hours) in the range from 773 K to 873 K (500 °C to 600 °C) has been carried out. The sequence of precipitation of secondary phases, their mass fraction, and coarsening rate have also been computed using JMatPro for both the steels. The average hardness values of the two steels after aging for different durations of time and temperature are tabulated in Table III. No significant change is observed contrary to the expected softening due to recovery. This could possibly be due to the compensation of reduction in hardness due to recovery by an

Table III.   Hardness (Macro-VHN) of RAFM Steels After Aging at 773 K to 823 K (500 °C to 550 °C)

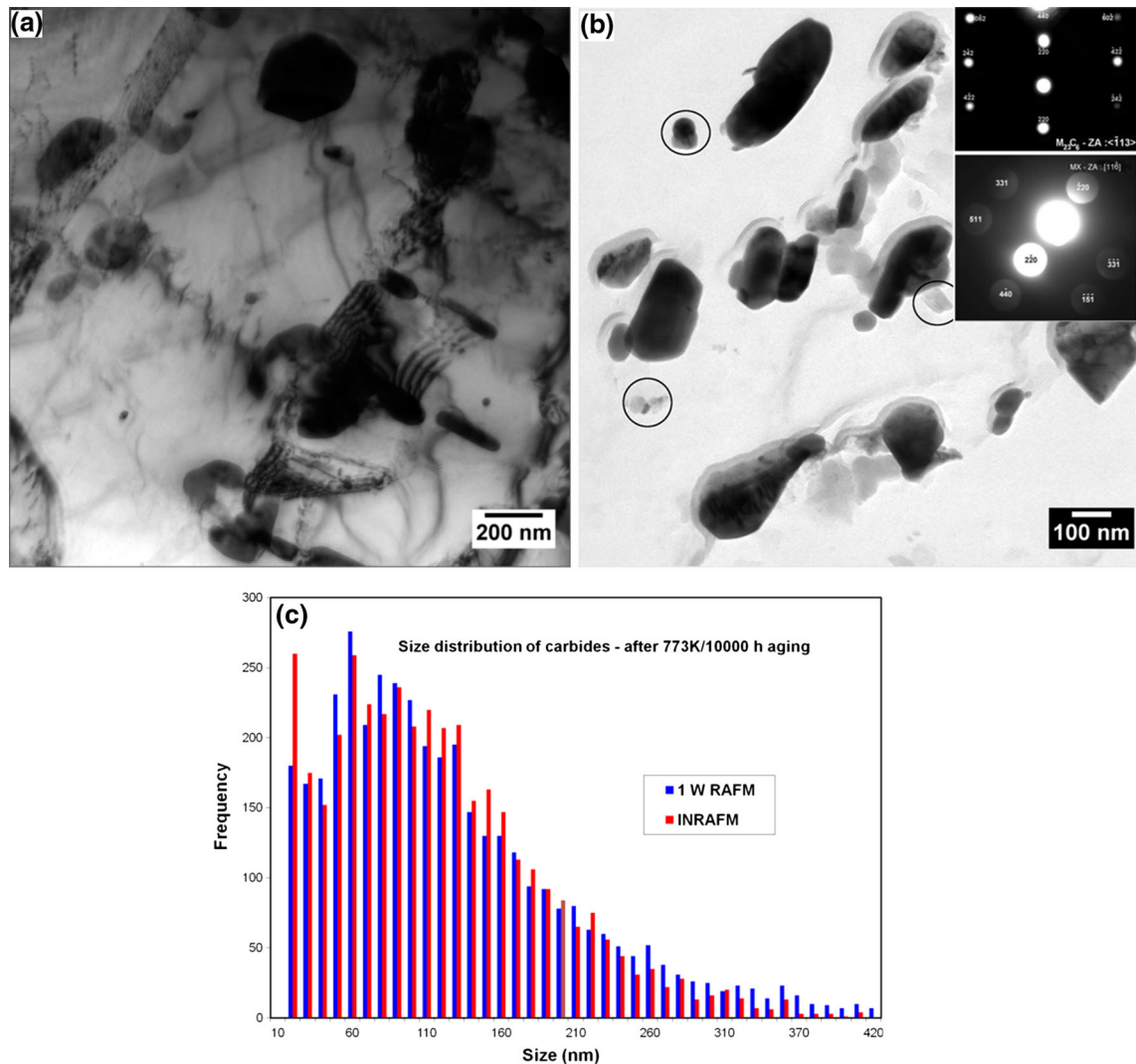| Steel	n & t	773 K (500 °C) /5000 h	773 K (500 °C)/10,000 h	823 K (550 °C) /5000 h	823 K (550 °C) /10,000 h
1 W steel	221 ± 5	220 ± 5	226 ± 5	223 ± 5	225 ± 5
INRAFM	230 ± 5	225 ± 5	225 ± 5	226 ± 5	224 ± 5

Fig. 7—TEM micrographs of steel aged at 773 K (500 °C) for 10,000 h showing (*a*) dislocation structure and coarsening of carbides in INRAFM steel (*b*) presence of coarse $M_{23}C_6$ carbides and fine MX (circled) carbides in 1W RAFM steel (inset—diffraction pattern from $M_{23}C_6$ and MX carbides along $\langle \bar{1}13 \rangle$ and $\langle 11\bar{6} \rangle$ zone axes, respectively) (*c*) comparison of size distribution of carbides.

increase due to precipitation. No significant change was observed in the microstructure of the two steels on aging for 5000 hours at 773 K (500 °C) except for a small increase in the size of the carbides. As the duration was increased to 10,000 hours, the steels retained the lath morphology, similar to the normalized and tempered steel, although few regions of low dislocation density and coarse precipitates (Figures 7(a) and (b)) were observed. Diffraction studies (inset of Figure 7(b)) confirmed the presence of both $M_{23}C_6$ and MX-type carbides. The increase in carbide size (Figure 7(c)) was more prominent for 1 W steel, where the maximum size

increased from 150 to 250 nm but was negligible in INRAFM steel.

As the temperature was increased to 823 K (550 °C), the extent of recovery as well as coarsening of precipitates increased in both the steels. The microstructural details of INRAFM steel aged for 5000 hours at 823 K (550 °C) are shown in Figure 8. TEM images at high magnification confirmed that the maximum size of carbide was of the order of 350 nm. As expected coarsening of $M_{23}C_6$ was less prominent in INRAFM steel than in 1 W steel in line with the higher amount of W, which resists coarsening, although the volume
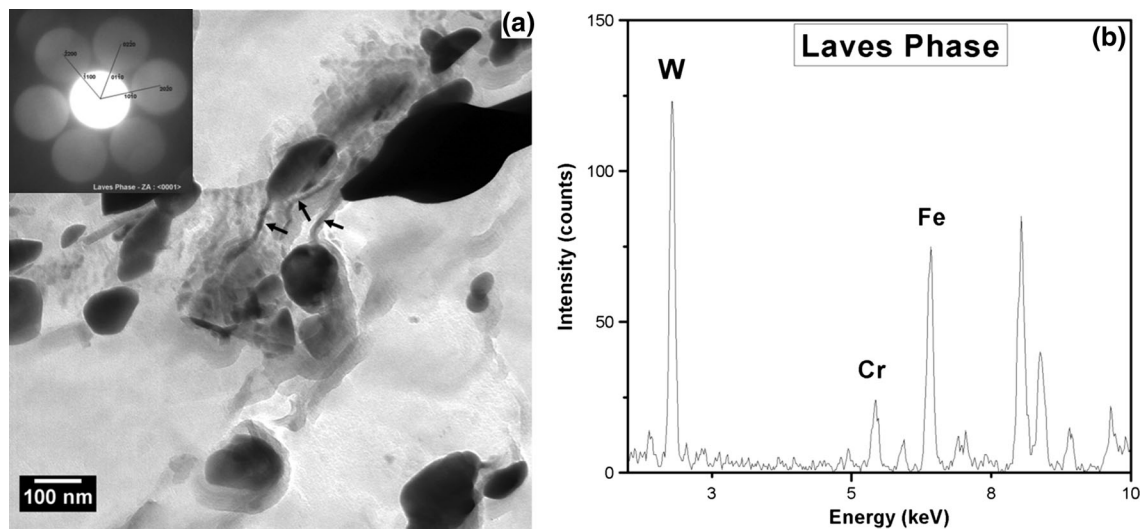
Fig. 8—TEM images of INRAFM steel aged for 5000 hours at 823 K (550 °C) (*a*) bright-field images of extraction replica showing fine lamellae of Laves phase (arrow marked) surrounding the lath boundary carbides (inset—diffraction pattern confirming the presence of Laves phase) (*b*) EDX spectrum revealing the enrichment of W and Fe in Laves phase.

percentage of carbides was higher for reasons explained earlier.[6,21,22] A high-magnification view of INRAFM steel in Figure 8(a) shows the presence of fine (~20 nm) lamellar features surrounding the coarse lath boundary carbides., Analysis of the diffraction pattern (inset—Figure 8(a)) obtained from the lamella identified it as Laves phase, rich in W and Fe with some solubility for Cr, corresponding to (Fe,Cr)$_2$W (Figure 8(b)). The average composition of this phase was measured as 59 pct W, 32 pct Fe, and 9 pct Cr. No evidence for Laves phase was found in the 1 W steel, despite a high enrichment of Cr in M$_{23}$C$_6$ carbides as compared to INRAFM steel. A small increase in the average microhardness value to 245 VHN was obtained unlike in the case of 773 K (550 °C).

As the aging time was increased to 10,000 hours at 823 K (550 °C), the microstructure of INRAFM steel (Figure 9) showed considerable changes. Although few regions maintained the lath morphology (Figure 9(a)) with broader laths [(~650 nm) and partially recovered grain structure, several other regions (Figure 9(b)] showed a high degree of recovery, partial recrystallization, and abundant precipitation. The distribution of M$_{23}$C$_6$ carbides along lath boundaries was maintained during coarsening of laths as shown in Figure 9(a). This suggests that dissolution and re-precipitation of carbides at lath boundaries take place in a cyclic manner during advancement of lath boundaries by boundary migration. Figures 9(c) and (d) show the distribution of carbides and preferential nucleation sites of Laves phase. From the comparison of Figures 8(a) and (d), it is understood that the Laves phase nucleates in the vicinity of lath boundary carbides after aging for 5000 hours at 823 K (550 °C) and grows in size to 30 to 40 nm on prolonged aging for 10,000 hours. Size distribution of carbides in 1 W and INRAFM steels aged for 10,000 hours at 823 K (550 °C) is shown in Figure 9(e). Although the average size is around 50 to 150 nm, a large number of coarse precipitates (600 to

700 nm) with Cr (~65 wt pct) characteristic of M$_{23}$C$_6$ carbides were observed in INRAFM steel. The average size of the *V*/Ta-rich MX phase remained stable at 30 to 40 nm even after aging for 10,000 hours, which therefore continue to provide creep strength to the steel.

The X-ray maps from carbon extraction replica given in Figure 10 clearly distinguish the W and Fe-rich (lean in Cr) Laves phase from the Cr-rich carbides. This suggests that Laves has nucleated in the vicinity of carbides and coarsened by the advantage of surface energy provided by carbides leading to the encapsulation of carbides. An overestimation of size (600 to 700 nm) and volume fraction of carbides in INRAFM steel at 823 K (550 °C) cannot be ruled out as the carbides are encapsulated by Laves phase. The observed precipitation behavior in the indigenous steels is in agreement with the reports on the Japanese low-activation ferritic-martensitic steel.[21,23–25]

E. *Simulation of Equilibrium Phases in Thermally Exposed RAFM Steels*

The sequence of evolution of secondary phases in 1 W and INRAFM steels as a consequence of thermal aging at 773 K (500 °C) and 823 K (550 °C) for duration in the range from 1 to 10,000 hours has been computed using JMatPro simulation software. The type and weight fraction of the different phases that form as a function of aging time at different temperatures have been determined. The predicted equilibrium phases at different temperatures are listed in Table IV, and the calculated weight fraction of carbides is given in Table V. As seen from the computation results, the weight percent of carbides in both the steels comes to saturation after 100 hours at both the temperatures. The volume fraction obtained from carbon extraction replica technique is given in Figure 11 for comparison. Since the density values of steel (7.8 × 10^3 Kg/m^3) and M$_{23}$C$_6$ (6.95 × 10^3 Kg/m^3) are not very different it is
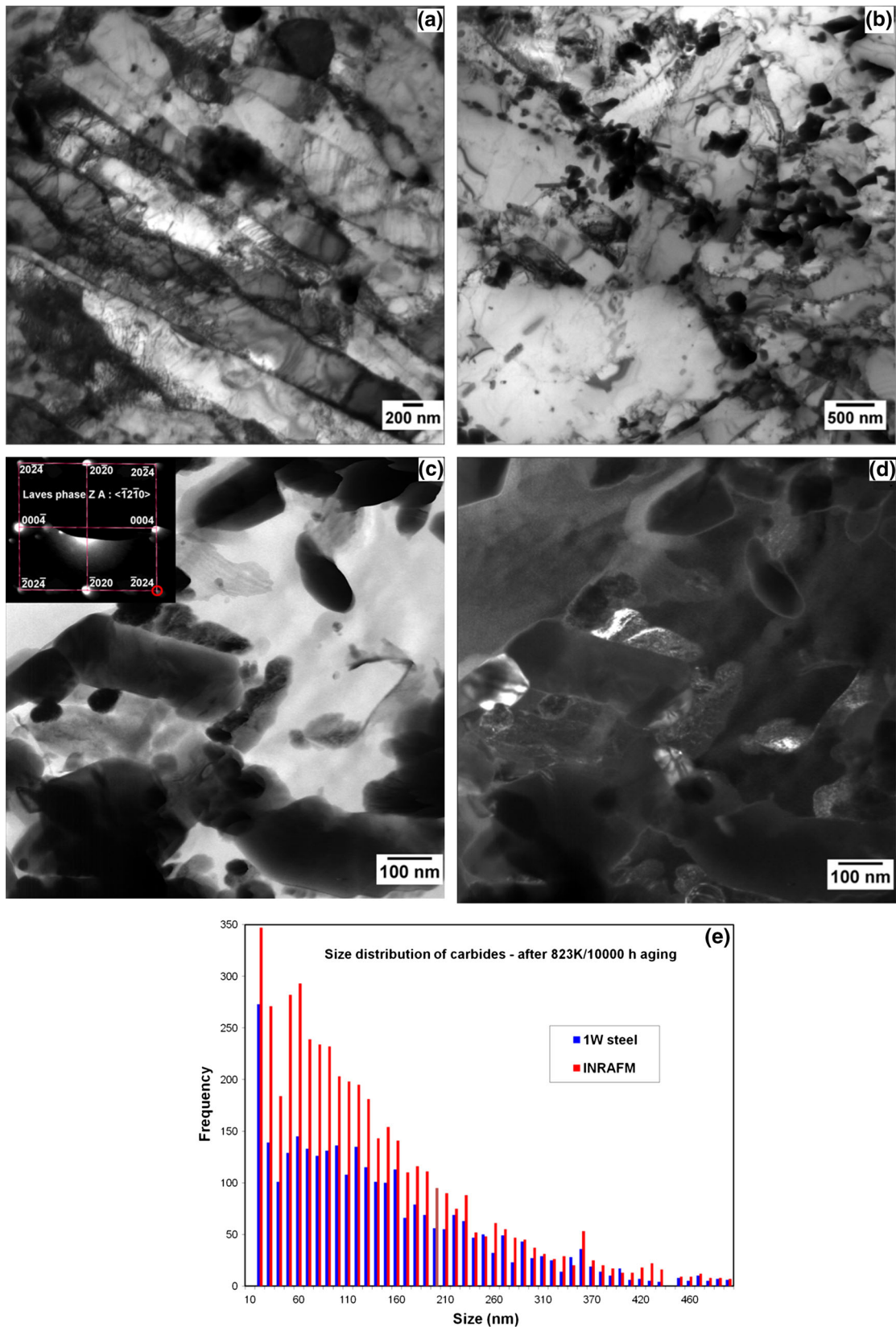
Fig. 9—Microstructure of INRAFM steel in steel aged for 10,000 hours at 823 K (550 °C) showing (*a*) retention of lath structure (*b*) well-recovered regions with coarse precipitates (*c*) BFI of carbides and Laves phase with inset showing diffraction patterns obtained from Laves phase along $\langle 1\bar{2}10 \rangle$ (*d*) dark field image highlighting the distribution of Laves phase using $\langle \bar{2}024 \rangle$ reflection marked in the diffraction pattern in (*c*) and (*e*) size distribution of the carbides in 1 W and INRAFM steels.
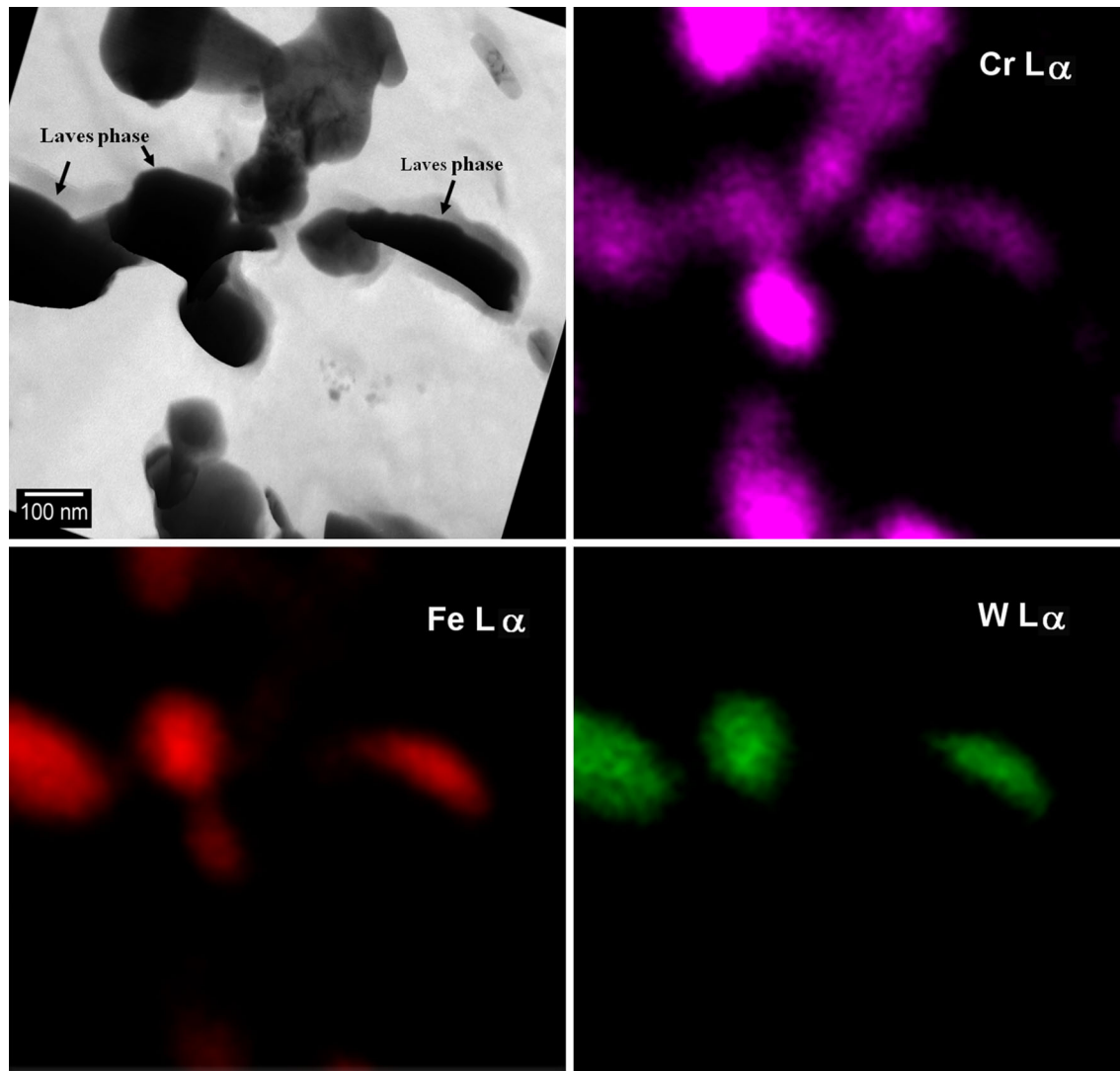
Fig. 10—X-ray map depicting the distribution of Cr, Fe, and W in the carbides and Laves phase.

Table IV. Simulated Sequence of Precipitation of Secondary Phases in 1 W and INRAFM Steels at Different Temperatures

	1 W		INRAFM	
Time (h)	773 K (500 °C)	823 K (550 °C)	773 K (500 °C)	823 K (550 °C)
1	M_7C_3, $M_{23}C_6$, M_3C, M_2X	$M_{23}C_6$, M_2X, M_7C_3	M_7C_3, $M_{23}C_6$, M_3C, M_2X	$M_{23}C_6$, M_2X, M_7C_3
100	$M_{23}C_6$, M_2X	$M_{23}C_6$, MX	$M_{23}C_6$, M_2X	$M_{23}C_6$, MX
1000	$M_{23}C_6$, MX	$M_{23}C_6$, MX, Laves	$M_{23}C_6$, MX	$M_{23}C_6$, MX, Laves
5000	$M_{23}C_6$, MX	$M_{23}C_6$, MX, Laves	$M_{23}C_6$, MX	$M_{23}C_6$, MX, Laves
10,000	$M_{23}C_6$, MX	$M_{23}C_6$, MX, Laves	$M_{23}C_6$, MX	$M_{23}C_6$, MX, Laves

reasonable to compare the mass and volume fraction. Although the experimentally determined values (Figure 11) are relatively higher than simulated values due to reasons explained in Section II, the trends are consistent. The replica analysis showed that volume fraction of carbide is high in INRAFM steel after aging, though there is no measurable difference in the maximum size of the carbide between the two steels. A

systematic increase in the volume fraction of carbides is observed as a function of time and temperature in both the steels. A relatively higher amount of precipitates in INRAFM in comparison to 1 W steel is clearly due to higher C content of the steel. The experimental values are in agreement with the simulated results except in the case of INRAFM steel aged at 823 K (550 °C) for 10,000 h. The sudden increase in the volume fraction of

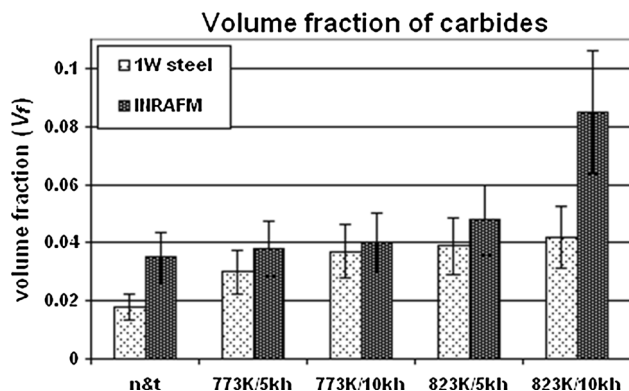| T	Time (h)	$M_{23}C_6$ (M_7C_3)		MX	
		1 W Steel	INRAFM	1 W Steel	INRAFM
773 K (500 °C)	1	0.0025 (0.01)	0.0038 (0.013)	—	—
	100	0.017	0.027	—	—
	1000	0.017	0.027	0.0004	0.0005
	5000	0.017	0.027	0.0007	0.0008
	10,000	0.017	0.027	0.0007	0.0008
823 K (550 °C)	1	0.015 (0.0003)	0.023 (0.001)	—	—
	100	0.017	0.03	0.0005	0.0005
	1000	0.017	0.03	0.0008	0.0009
	5000	0.017	0.03	0.0008	0.0009
	10,000	0.017	0.03	0.0008	0.0009

Fig. 11—Estimation of volume fraction of carbides in aged 1 W and INRAFM steels.

carbides in 823 K (550 °C)/10,000 hours could be due to the overestimation caused by the presence of Laves phase during image analysis.

The computed change in the size of $M_{23}C_6$ and MX carbides is plotted as a function of aging time for various temperatures in Figures 12(a) and (b) for the two steels. The increase in mean size of $M_{23}C_6$ carbides during aging follows the Ostwald ripening mechanism, since the super-saturation of carbon in the martensite is relieved by precipitation primarily during tempering or early stages of aging. This is consistent with the observed increase in size of the carbide with no increase in weight percentage, Table V. In INRAFM steel, the $M_{23}C_6$ carbides with high W concentration show a slower kinetics of coarsening on aging and the apparent increase in size is due to the encapsulation of Laves phase on carbide. It is well known that the carbides on lath boundaries resist the coarsening of laths, whose effect reduces as the carbides coarsen. The difference in amount and size between computed and experimental results in INRAFM steel on aging for 10,000 hours at 823 K (550 °C) is mainly due to the additional precipitation of Laves phase surrounding the carbides. Microchemical analysis of $M_{23}C_6$ precipitates is presented in Figure 12(c). A progressive increase in the Cr and W contents in $M_{23}C_6$ is observed with time in both the steels. There is also a large variation in the Cr and W contents, which is attributed to the simultaneous coarsening and fresh nucleation of carbides during thermal exposure.

Following are the significant differences in the predicted behavior of microstructural evolution between the INRAFM and 1W steels at high temperatures:

- Higher fraction of secondary phases in INRAFM steel than 1 W steel at all conditions.
- Early onset of precipitation of MX carbides specifically at 823 K (550 °C).
- M_2X carbonitrides are stable at the early stages of heat treatment.
- Formation of Laves phase in both the steels after 1000 hours of aging at 823 K (550 °C), with relatively higher weight percentage (V_f^{LP}) in INRAFM steel ($V_f^{INRAFM} = 0.003$) than in 1 W steel ($V_f^{1 W} = 0.001$).
- Laves phase was the second most predominant phase ($V_f^{LP} = 0.228$) next to $M_{23}C_6$ ($V_f^{M_{23}C_6} = 2.7$) after aging for 5000 hours at 873 K (550 °C).

As expected, coarsening rate of MX carbides in both the steels was found to be much lower than that of $M_{23}C_6$. In addition, the average size of the MX precipitates in INRAFM steel was lower than that in 1 W steel. The computation was carried out by adopting a uniform composition of the steel, which is true for a martensite structure as in normalized condition. The effect of tempering is not incorporated in the computation due to the limitation of the software. Computation gives the maximum attainable size of the carbide at a particular temperature where as the actual experimental values reflect a wide distribution.

IV. DISCUSSIONS

The influence of aging on the creep deformation behavior has been discussed in detail in Section III–C, correlating the corresponding microstructures. Both 1 W and INRAFM steels showed a tempered martensitic structure consisting laths decorated with inter- and intra-lath carbides. The higher volume fraction of carbides in INRAFM steel compared to 1 W steel is understood on the basis of higher carbon content in the steel. Computation showed that the dissolution
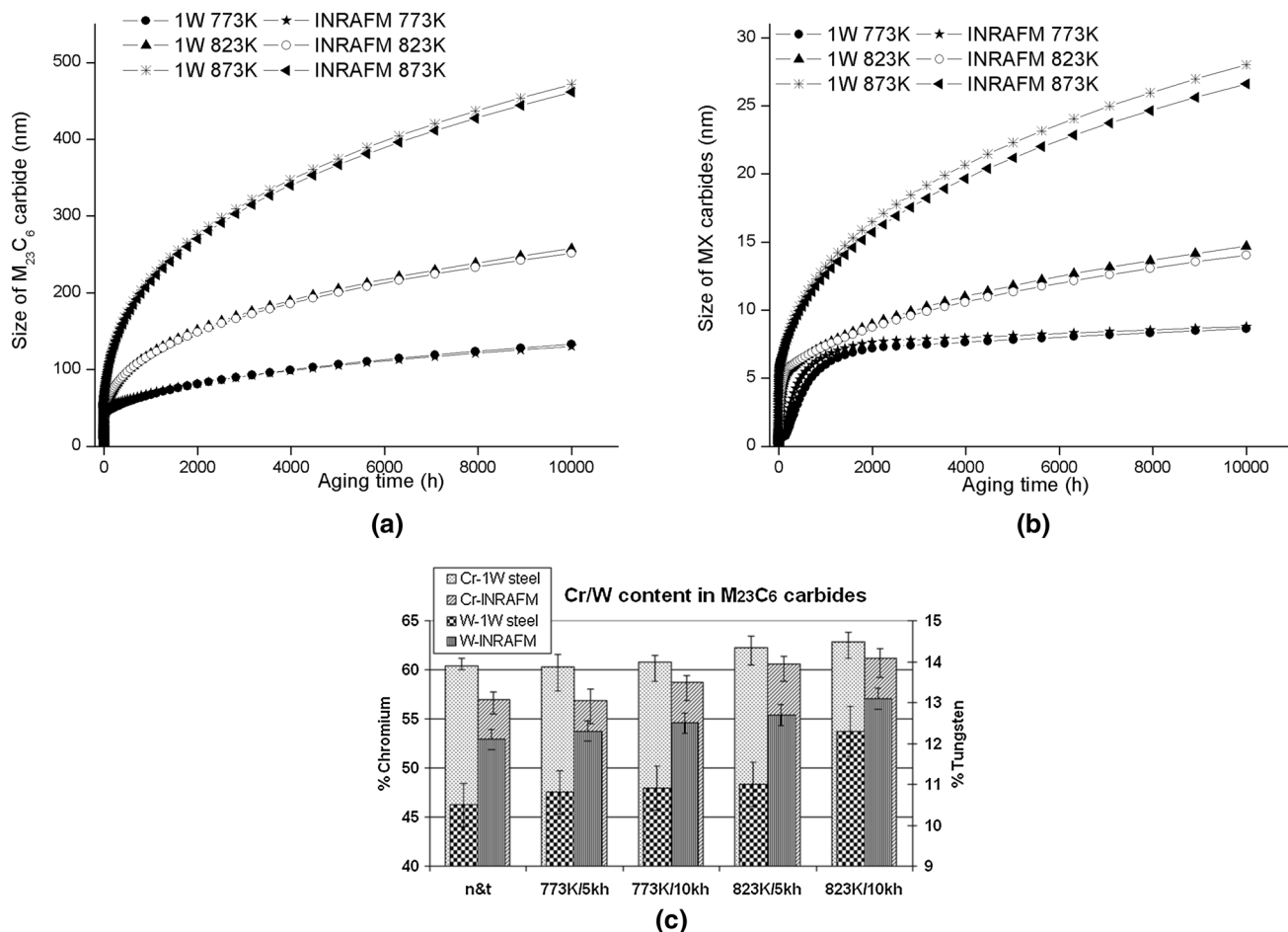
Fig. 12—Precipitate characteristics as a function of aging temperature and time in INRAFM steels. (*a* & *b*) Precipitate size (JMatPro simulated) of $M_{23}C_6$ (*a*) and MX (*b*); (*c*) Cr and W contents in $M_{23}C_6$ (experimental).

temperature of $M_{23}C_6$ in INRAFM steel is higher as compared to 1 W steel and the pinning of grain boundaries by the carbides at austenitizing temperature is responsible for the fine PAGS of INRAFM steel.

In the secondary creep region, both work hardening and recovery are in balance resulting in a steady-state creep. Ferritic steel unlike austenitic steel does not show a distinct transition from transient to secondary creep during a conventional creep test. This is because the initial microstructure of ferritic steel that evolved during tempering of martensite has a high dislocation density with limited work-hardening capability and hence recovery is more dominant. Thus, the normalized and tempered 1 W and INRAFM steels did not exhibit distinct primary stage. However, results showed that an increase in 0.4 pct W in INRAFM steel decreases the creep rate to nearly half the value of 1 W steel. Since, dislocation climb plays a major role in creep deformation, as it aids the recovery of excess dislocations and requires diffusion of vacancies and interstitials, the rate controlling step is atomic diffusion.

The role of W on diffusivity is very well known and its effect on substructure is already discussed in Section III–A. The presence of W not only reduces the lath size but also resists the coarsening of laths. Coarsening of laths is associated with recovery of dislocations and coarsening of carbides. Studies on Fe-Cr-W alloys showed that W strikingly reduces the rate of self-diffusion of Fe, while the effect of Cr is not significant.[21,26] Recovery of dislocation involves self-diffusion of Fe and coarsening of carbides depends on its stability. Hence, in both ways, W resists recovery process, which is reflected by the higher creep strength. It is reported that for a 9Cr-0.5Mo-W steel, both tensile and creep rupture strength increase with increasing W content.

All thermally aged steels showed a distinct primary creep stage unlike normalized and tempered steel. This phenomenon can be attributed to the softening caused by recovery. The softening is primarily a result of the coarsening or dissolution of the carbides, which in turn result in recovery of dislocation substructures. During creep test, the softer matrix undergoes work hardening to a greater extent as compared to the normalized and tempered steel. The increase in creep rate (or decrease in creep strength) in the steel aged at 773 K (500 °C) can be understood on the basis of above-mentioned reasons. The impression creep rate remained almost the same in the steel aged for longer times of 10,000 hours. This can be understood in terms of the nearly same amount of precipitation (Table V) with time of aging.

The nucleation of fine Laves phases after aging for 5000 hours at 823 K (550 °C) also manifested as a small increase in the average microhardness value to 245 VHN. The high density of precipitates is considered to be responsible for the delayed recovery of lath structure in W-containing steels. INRAFM steel aged at 823 K (550 °C) for 5000 hours showed the lowest creep rate or highest creep strength among all the aged steel, despite the higher substructure changes expected on exposure to higher temperature. This is clearly ascribed to the existence of the Laves phase that formed at 823 K (550 °C) as shown in Figures 4 and 8. The presence of uniformly distributed nano-sized particles of Laves phase is responsible for the increase in creep strength. This is in agreement with the earlier studies carried out by other researchers in similar steels.[20,27]

The nucleation of Laves phase as a thin layer along the lath boundaries in the vicinity of coarse carbides is in agreement with the earlier reports. Sawada *et al.* reported that the lath boundaries are the preferential site of nucleation of Laves phase in W-containing steel because of which the number density of precipitates in the lath boundary increases.[27] It is understood that the coarse carbides consume large amounts of Cr and C, leaving the surrounding matrix depleted in Cr resulting in a localized enrichment of W, which favors the nucleation of Laves phase, provided there is enough thermodynamic driving force for its formation. However, an increase in aging time (10,000 hours) at 823 K (550 °C) increased the creep rate to nearly that at 773 K (500 °C)/5000 hours. The precipitation of Laves phase leads to a depletion of W in the matrix and to a reduction of the solid solution-hardening effect in alloys.[10,14,28] On the other hand, Laves phase precipitation can contribute to precipitation hardening and a resultant increase in the creep strength before it coarsens.

Murata *et al.* and John Hald *et al.* have determined the interfacial energy of Laves phase in similar systems and report that fine Laves phase has low interfacial energy (0.1 J/m^2) which increases to 0.8 J/m^2 as it coarsens.[29,30] An interfacial energy in the range from 0.8 to 1 J/m^2 indicates incoherent interfaces between Laves phase and ferrite. Also, their results indicate a morphological change of the phase from fine coherent to granular precipitates. A similar morphological change observed in Figure 10 also points to the fact that they are incoherent with ferrite.

The Laves phase during aging at 823 K (550 °C) for 10,000 hours not only coarsens but also forms as a discontinuous net work along the lath and grain boundaries. This network of a brittle phase reduces the strength of the interface, which is well reflected in the results of impression creep tests (exhibited higher penetration rate). It is predicted that further exposure at this temperature may result in a continuous network of Laves phase along the boundaries. Hence the increased creep rate of the INRAFM steels at 823 K (550 °C) after 10,000 hours is attributed to the higher extent of recovery and the coarsening of Laves phase.

Even though JMatPro computations indicated the formation of low amounts of Laves phase in 1 W steel, no experimental evidence was obtained for its presence due to lower content of tungsten in the matrix. Precipitation of Laves phase has been reported earlier in the HAZ of F82H (8Cr-2WVTa) steel after thermal aging at 823 K (550 °C) for 3000 hours.[31] Compared to 1 W steel, formation of Laves phase occurred early in INRAFM steel due to higher W content and abundant precipitation of carbides that increased the availability of W and reduced the super-saturation of carbon.

V. CONCLUSIONS

A detailed microstructural characterization of normalized and tempered RAFM steels with two different W contents has been carried out. Microstructural features determined by experiments and computation are compared. Evolution of microstructure was studied with respect to coarsening of carbides and formation of Laves phase. Impression creep tests have been carried out to evaluate difference in creep strength of the two steels. The important results are summarized as follows:

- Normalized and tempered RAFM steel possess a tempered martensitic structure consisting of ferrite and carbides, retaining lath morphology of the martensite.
- Carbides were identified as Cr-rich $M_{23}C_6$ and *V*/Ta-rich MX carbides.
- Higher W content in INRAFM steel resisted the coarsening of $M_{23}C_6$ carbides.
- Coarsening of MX was negligible in both steels.
- A progressive enhancement of Cr is observed in the $M_{23}C_6$ upon aging, supported by computation on equilibrium phases.
- Although computation predicts the nucleation of Laves phase during at 773 K (500 °C) in 1W steel, no experimental evidence could be obtained even after 10,000 hours of aging which is due to kinetic factors.
- Increase in W content improved the creep strength of the steel in the normalized and tempered condition.
- Laves phase nucleates at a temperatures of 823 K (550 °C) in INRAFM steel and this improved the creep strength for the steel aged up to 5000 hours
- Aging beyond 10,000 hours resulted in discontinuous network of Laves phase, which deteriorated the creep strength of the steel.

REFERENCES

1. R.L. Klueh and D.R. Harries: *High-Chromium Ferritic and Martensitic Steels for Nuclear Applications*, ed. ASTM. vol. ASTM MONO3. 2001.

2. M. Tamura, K. Shinozuka, K. Masamura, K. Ishizawa, and S. Sugimoto: *J. Nucl. Mater.*, 1998, vols. 258–263 (Part 2), pp. 1158–62.

3. C.R. Brinkman, B. Gieseke, and P.J. Maziasz:The influence of long term thermal aging on the microstructure and mechanical properties of modified 9Cr-1Mo steel in *Microstructures and Mechanical Properties of Aging Material*, R. Viswanathan P.K. Liaw K.L. Murty E.P. Simonen D. Frear , eds., The Minerals, Metals & Materials Society, Orlando, 1993, pp. 107–16.

4. S. Saroja, M. Vijayalakshmi, and V.S. Raghunathan: *Mater. Trans. JIM*, 1993, vol. 34 (10), p. 901.

5. F. Abe: *Metall. Mater. Trans. A*, 2005, vol. 36A, pp. 321–32.

6. S.G. Hong, W.B. Lee, and C.G. Park: *J. Nuc. Mater.*, 2001, vol. 288, pp. 202–07.

7. J. Cermak, J. Kucera, and B. Million: *J. Krumpos: Kov. Mater.*, 1980, vol. 18, p. 537.

8. R. Mythili, J. Ravikirana, K. Vanaja, S. Laha, T. Saroja, M.D. Jayakumar, and E.Rajendrakumar. Mathew: *Proc. Eng.*, 2013, vol. 55, pp. 295–99.

9. L.J. Seung, A.H. Ghassemi, M. Kouichi, M. Taro, and A. Hitoshi: *Mater. Sci. Eng. A*, 2006, vol. 428 (1–2), pp. 270–75.

10. C.G. Panait, W. Bendick, A. Fuchsmann, and A.F. Gourgues-Lorenzon: *J. Besson: Int. J. Press. Vessel. Pip.*, 2010, vol. 87 (6), pp. 326–35.

11. K. Laha, S. Saroja, A. Moitra, R. Sandhya, M.D. Mathew, T. Jayakumar, and E. Rajendrakumar: *J. Nucl. Mater.*, 2013, vol. 439, pp. 41–50.

12. F. Abe: *Mater. Sci. Eng.*, 2004, vols. 387–389, pp. 565–9.

13. R. Lindau and M. Schirra: *Fusion Eng. Des.*, 2001, vols. 58–59, pp. 781–5.

14. T. Hasegawa, Y.R. Abe, Y. Tomita N. Maruyama M. Sugiyama: *ISIJ Int.*, 2001, vol. 41 (8), pp. 922–9.

15. T. Mukherjee, W.E. Stumpf, and C.M. Sellars: *J. Mater. Sci.*, 1968, vol. 3 (2), pp. 127–35.

16. U.R. Kattner: *JOM*, 1997, vol. 49 (12), pp. 14–19.

17. H.L. Lukas, J. Weiss, and E.-T. Henig: *CALPHAD*, 1982, vol. 6, pp. 229–51.

18. V.D. Naveena, V. Vijayanand, K. Ganesan, M.D. Laha, and M.D. Mathew: *Mater. Sci. Technol.*, 2014, vol. 30 (10), pp. 1223–28.

19. V. Thomas Paul, C. Sudha, and S. Saroja: *Metall. Mater. Trans. A*, 2015, vol. 46A, pp. 3378–92.

20. J. Hald: *Steel Res.*, 1996, vol. 67 (9), pp. 369–74.

21. F. Abe, H. Araki, and T. Noda: *Metall. Mater. Trans A*, 1991, vol. 22A, pp. 2225–35.

22. S. Ghosh: *J. Mater. Sci.*, 2010, vol. 45 (7), pp. 1823–29.

23. Y. Hosoi, N. Wade, S. Kunimitsu, and T. Urita: *J. Nucl. Mater.*, 1986, vols. 141–143, pp. 461–67.

24. G. Dimmler, P. Weinert, E. Kozeschnik, and H. Cerjak: *Mater. Charact.*, 2003, vol. 51 (5), pp. 341–52.

25. L. Korcakova, J. Hald, and M.A.J. Somers: *Mater. Charact.*, 2001, vol. 47 (2), pp. 111–17.

26. A.W. Bowen and G.M. Leak: *Metall. Trans. A*, 1970, vol. 1 (6), pp. 1695–1700.

27. K. Sawada, M. Takeda, K. Maruyama, R. Ishii, M. Yamada, Y. Nagae, and R. Komine: *Mater. Sci. Eng. A*, 1999, vol. 267 (1), pp. 19–25.

28. F. Abe: *Mater. Sci. Eng. A*, 2001, vols. 319–321, pp. 770–73.

29. M. Yoshinori, K. Toshiyuki, M. Masahiko, and M. Toru: *ISIJ Int.*, 2002, vol. 42 (12), pp. 1423–29.

30. J. Hald and L. Korcakova: *ISIJ Int.*, 2003, vol. 43 (3), pp. 420–27.

31. T. Sawai, K. Shiba, and A. Hishinuma: *J. Nucl. Mater.*, 2000, vols. 283–287, pp. 657–61.